Finite Element Modelling and Optimization of the Occupant-Seat System for Predicting Seat Transmissibilities and the Cross-Axis Effect with Different Foam Thicknesses

Xiaolu Zhang

College of Mechanical & Energy Engineering, Beijing University of Technology, Beijing, China.
Engineering Research Center of Advanced Manufacturing Technology For Automotive Components, Ministry of Education, Beijing University of Technology, China.

Xiangyu Chen, Yuxin Gao, Yuanfei Duan and Yang Miao

College of Mechanical & Energy Engineering, Beijing University of Technology, Beijing, China.
E-mail: ymiaoi@163.com

(Received 09 September 2025; accepted 28 January 2026)

The variation of the open-cell polyurethane foam thickness within the seating system can affect the dynamic response of the occupant-seat system and the riding discomfort. This study was aimed to develop and optimize a finite element model of the occupant-seat system incorporating the skeleton and muscle tissue for predicting the seat transmissibility and assessing the riding discomfort with different foam thicknesses. The key model parameters influencing the prediction of the seat transmissibility were investigated with the sensitivity analysis, and the correlation between the parameters and the seat transmissibilities was quantified by fitting the polynomial functions. The genetic algorithm was also utilized to iterate the squared error between the predicted and the measured seat transmissibilities, thereby obtaining the optimal parameter values. The best fit of the vertical in-line and fore-and-aft cross-axis seat transmissibility predicted by the optimized model increased by 13.34 % and 14.41 %, respectively. When the dynamic stiffness of the foam decreased with the increase of the thickness, the peak frequency of seat transmissibilities, the weighted root-mean-square acceleration and the SEAT value exhibited the same downward trend.

NOMENCLATURE

WRMSA	weighted root-mean-square acceleration
SEAT	seat effective amplitude transmissibility
SE	squared error

1. INTRODUCTION

Vehicle vibrations can influence human health and riding comfort.[1,2] The vibration transmission through the occupant-seat system is affected by both the seating dynamics and the biodynamics of the human body.[3] The seat transmissibility can be? to quantify the overall dynamic response of the system, and it can be calculated based on the input vibration at the seat base and the responses at the occupant-seat interfaces.[4,5] The seat transmissibility also exhibited the pronounced cross-axis effect (the vibration in one direction can induce the vibration along the orthogonal axis).[5,6]

Vibrations can be attenuated by the open-cell polyurethane foam of the seat system.[7] The low-density foam exhibited a more even distribution of the contact pressure compared to the high-density foam, thereby improving the static riding comfort.[8] The foam with high density dampened vibration faster than that with low density.[9] Furthermore, the peak transmissibility of the seat transmissibility decreased with decreasing the foam density and increasing the foam stiffness,[9] and the peak frequency of the seat transmissibility decreased with increasing the foam hardness10. The dynamic stiffness of the polyurethane foam was also associated with factors such as the foam thickness, vibration magnitudes and preloads. It is necessary to model and validate the hyper-elastic property of the foam, thereby improving the predictive performance of the occupant–seat model.

The biodynamic response of the human body is commonly quantified by the apparent mass. The peak frequency of the vertical in-line apparent mass decreased when increasing the vibration amplitude.[4] Furthermore, the peak frequency was correlated with the vibration modes.[11,12] The vibration modes were mainly characterized by the pitching movement and the vertical movement of the human body during the exposure to the vertical vibration.[13] The vibration modes can be simulated to further analyze the movement tendency of the human body model, thereby validating the capability of predicting the cross-axis effect of the occupant-seat system.

Various models have been built to explore the static and dynamic characteristics of the occupant-seat system. Lumped parameter models are constructed with lumped masses, springs and dampers. Yet the simplicity in the model structure poses challenges in capturing the cross-axis responses in the system.[14] Multi-body models are characterized by increased degrees of freedom and additional components such as ball joints, enabling detailed analysis of the rotations of the system.[15] Nevertheless, both the multi-body and lumped param-

eter models still possess limitations in analyzing the geometry characteristics, the material properties and the contact. The pressure distribution at the occupant-seat interface is also difficult to investigate for evaluating the riding comfort.

Finite element models incorporate the detailed geometry so as to model the anatomical structures and the complex contours. The local static pressure distribution could be simulated by the buttocks model,[16–18] while the dynamic occupant–seat interactions were hardly reflected. The vertical in-line seat transmissibility could be predicted by the human body model incorporating the skeletal structure, while the fore-and-aft cross-axis vibration modes were seldom captured.[19] The vertical in-line apparent mass was predicted utilizing the model including the ischium and the femur, while the vibration modes near the resonance frequency were not simulated due to the absence of the spine.[20] Therefore, the capability of simulating vibration modes can be enhanced by developing the human body model including the skeleton (e.g., the ischium and the spine), thereby improving the capability of predicting seat transmissibilities and the cross-axis effect.

The weighted root-mean-square acceleration (WRMSA) and the seat effective amplitude transmissibility (SEAT) proposed in the ISO 2631-1 can be further computed to assess the predictive accuracy of the model and the riding discomfort. Compared with sitting conditions on a rigid seat, the SEAT value and the WRMSA decreased significantly when the low-hardness open-cell polyurethane foam cushion was adopted.[21,22] Furthermore, both indicators decreased with increasing the vibration amplitude.[22] Therefore, the correlation between the SEAT value and the WRMSA with the foam thickness is worthy of further investigating in order to explore the influence of the foam thickness of the seat cushion on the riding comfort.

In this study, a finite element model of the occupant-seat system incorporating seat structures and certain parts of the human body (e.g., the pelvis and the spine) was constructed to explore the seat transmissibilities and the cross-axis effect with different foam thicknesses. The sensitivity analysis, the polynomial fitting and the genetic algorithms were utilized to adjust the key model parameters affecting the predictive accuracy of the seat transmissibility, and the weighted root-mean-square acceleration and the seat effective amplitude transmissibility were also evaluated.

2. MODELLING OF THE CAR SEAT

A seat model was developed and composed of the seat frame, rails, seat belt buckle, motor cables, rotary connection mechanism, the open-cell polyurethane foam block, etc. (Fig. 1 a). Since the computational efficiency was influenced by the model complexity, simplifications of the original seat model were carried out. The seat frame, rails, motor cables, bolts, and seat belt buckle were set as rigid body. The connection structures of the rotary connection mechanism were selectively retained and the rotational degree of freedom of the backrest was flexible. The 10 mm hexahedral elements were utilized to mesh the main body of the seat, while the tetrahedral elements were also utilized to mesh the irregular structures. The number of mesh elements in the original and simplified models was 309910 and 224384, respectively.

(a) Seat model

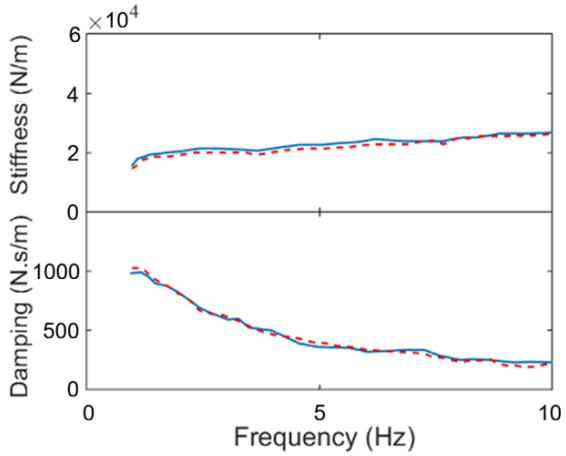

(b) The predicted and the measured stiffness: —test; - - -simulation

Figure 1. The seat model and the definition of the foam stiffness (foam thickness: 80 mm).

The density, the Poisson's ratio and the stiffness of the seat frame and the connection mechanism were set as 7800 kg/m^3, 0.3 and 210 GPa, respectively.[23] The foam properties were defined using the non-linear hyper-elastic model. The non-linearity was represented with the elastic strain-energy function W.[24,25] The parameterization of this model was obtained from the measurement of the uniaxial shear and compression tests. The parameters were set as: $a_1 = 164.86$ kPa, $m_1 = 8.88$, $m_2 = -4.82$, $n_1 = 0.0$, $n_2 = 0.0$, $a_2 = 0.0230$ kPa.

$$W = \sum_{i=1}^{N} \frac{2a_i}{m_i^2} \left[\hat{\lambda}_1^{m_i} + \hat{\lambda}_2^{m_i} + \hat{\lambda}_3^{m_i} - 3 + \frac{1}{n_i} \left((J^e)^{-m_i n_i} - 1 \right) \right]. \tag{1}$$

where N is the order of the polynomial, m_i, a_i and n_i are parameters dependent on temperature, $\hat{\lambda}_1 = (J^{th})^{-\frac{1}{3}} \lambda_i$, $\hat{\lambda}_1 \hat{\lambda}_2 \hat{\lambda}_3 = J^e$, λ_i is the principal displacement, and J^e is the volumetric strain rate.

The open-cell polyurethane model was validated by the dynamic stiffness from the measurement:

(i) The foam was positioned between the indenter head and the vibrator;

(ii) The indenter head descended until the pre-load force reached 600 N;

(iii) The vibrator applied the vertical random vibration (RMS acceleration magnitude: 0.4 ms^{-2}) to foam.

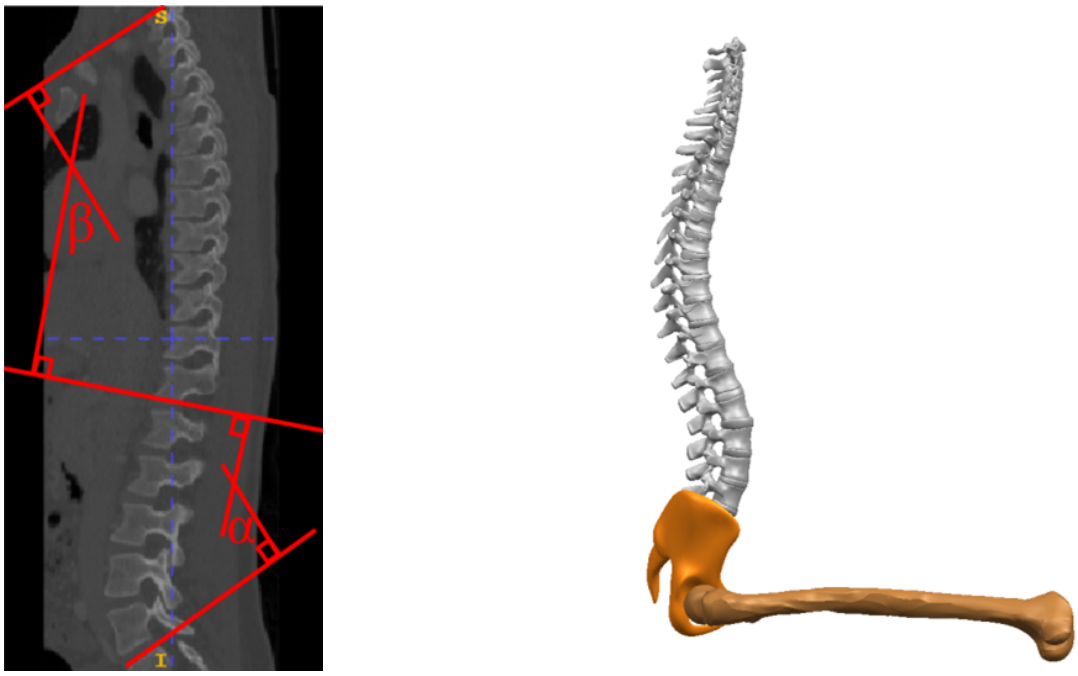

(a) Sagittal spine CT (b) Skeletal model

Figure 2. Setting of the spine model.

Table 1. Comparison of main parameters.

Main dimensions	Standard	This study
Height (cm)	175.4	175.6
Lower leg length (cm)	39.6	40.8
Thigh length (cm)	49.6	48.9
Fore arm length (cm)	25.3	24.5
Upper arm length (cm)	33.3	34.8

The comparison indicated a high consistency between the predicted and measured curves (Fig 1 b).

3. MODELLING OF THE SEATED HUMAN BODY

A human body model was constructed utilizing the anatomy data and the body measurement parameters provided by the GB 10000-88 Chinese Adult Body Size Standard (Table 1). The simplification and the merging of the original model were carried out. Since the prediction accuracy was almost unaffected by the limbs,[23,26] the hands were ignored, and the toes were merged as a single entity. Since the whole-body vibration was hardly influenced by the internal forces of organs, the viscera in the pelvis, the abdomen and the thoracic cavity were simplified as one part. To facilitate the material and the contact definitions of the model, this model was composed of five body segments: the leg-foot, the abdomen-thigh-pelvis, the arm, the thorax-shoulder, and the head-neck.

The dynamic response of the human body could be influenced by the skeleton.[13,25,27] Since the computational cost was influenced by the complexity of the skeletal model, simplifications were carried out as well. The pelvis and the femur were the primary parts in contact with the seat, and the pitch movements were observed in experiments.[13] Thus, the pelvis and the femur models were constructed based on the anatomical parameters (e.g., the pelvic width and the femur length). Furthermore, the vertical and the fore-and-aft movements of the human body were influenced by the spine.[25] The parameters of the lumbar, the thoracic and the cervical vertebrae (e.g. the vertebral height and the intervertebral disc thickness) were extracted to construct a spine model. The spine model was then modified to match the skeletal posture of the body in the seated position. ITK-SNAP software was utilized to analyze the CT-Spine1K dataset from the SpineWeb, and the spinal morphology of the human body was obtained. The vertebral arrangement, the lumbar curvature angle (α) and the thoracic curvature angle (β) were measured so as to set the angles and positions for the spine model (Fig. 2). The human body, the pelvis and the femur model were meshed using the 10 mm tetrahedral elements. As the spine model consisted of relatively small structures (e.g. the intervertebral discs and the vertebral bodies), various element sizes were attempted and the 1 mm element was selected (see Fig. 3). The mesh elements at the occupant-seat interfaces were adjusted and refined manually (see Fig. 4). The skeleton and the muscle tissues were assigned with different material properties. The density and the stiffness of the skeleton were set to 1700 kg/m^3 and 16.7 GPa, respectively. The density of the muscle tissues was defined as 1060 kg/m^3. The nonlinear behavior of the muscle tissues was defined with the Mooney-Rivlin model:[23]

$$U = X_1(Y_1 - 3) + X_2(Y_2 - 3) + X_3(Y_3^{-2} - 1) + X_4(Y_3 - 1)^2; \quad (2)$$

where Y_1, Y_2 and Y_3 represent the invariant quantities of the Cauchy-Green strain tensor, V:

$$V = P^T P; \quad (3)$$

$$Y_1 = \mathrm{trace}(V); \quad (4)$$

$$Y_2 = \frac{1}{2}\left[\mathrm{trace}^2(V) - \mathrm{trace}(V^2)\right]; \quad (5)$$

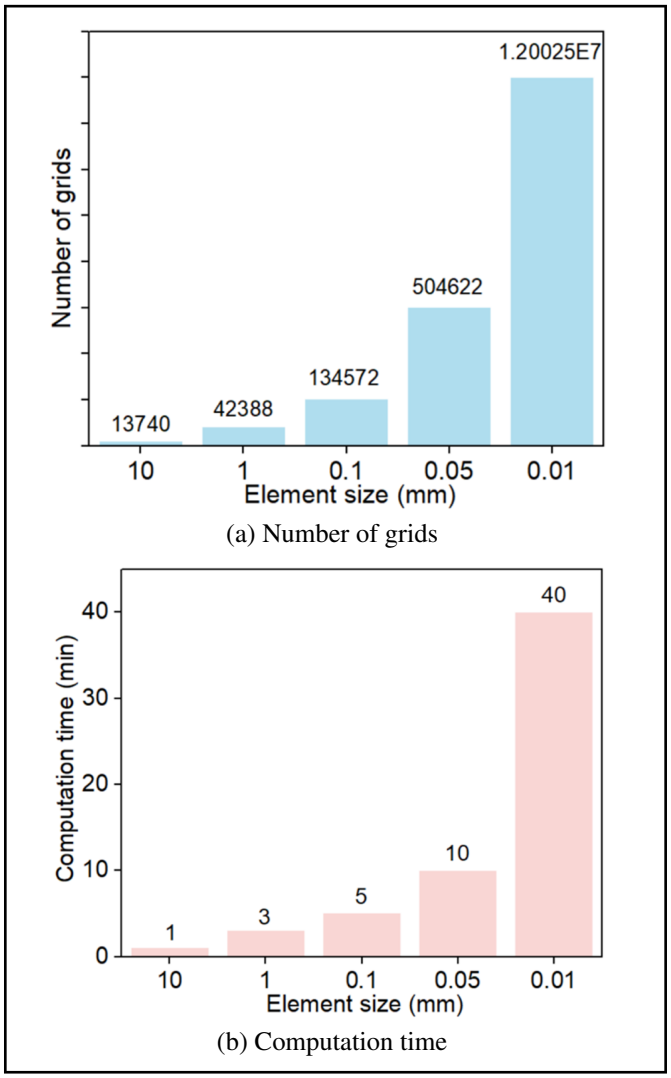

(a) Number of grids

(b) Computation time

Figure 3. The number of grids and computation time for different spine element sizes.

Table 2. The damping and stiffness of joints.

Joint	**Damping** (Nms/rad)	**Stiffness** (Nm/rad)
Thorax	9.8	2420.0
Waist	27.2	2080.0
Hip	21.3	536.0
Knee	280.6	280.0

$$Y_3 = \det(V); \tag{6}$$

$$X_3 = \frac{1}{2}X_1 + X_2; \tag{7}$$

$$X_4 = \frac{X_1(5v-2) + X_2(11v-5)}{2(1-2v)}; \tag{8}$$

where P is the deformation tensor. The parameters were set to: $v = 0.49$, $X_1 = 1.65$ kPa, $X_2 = 3.35$ kPa.[25] Furthermore, the main joints of the model included the thorax, waist, hip and knee joint (see Table 2). Four vibration modes were obtained from the model (Fig. 5). The first mode at 2.69 Hz involved the fore-and-aft movement of the head and the buttocks. The second mode at 4.70 Hz involved the fore-and-aft movement of the lower body and the bending of the spine. The third mode at 6.01 Hz involved the vertical movement of the whole body and the pitching movement of the pelvis. The fourth mode at 9.08 Hz consisted of the pitching movement of the pelvis and the vertical movement of the buttocks. The obtained vibration modes were consistent with previous studies,[11,13,28] indicating the fore-and-aft and the vertical vibration responses of the human body could be accurately represented by the calibrated model. These simulated vibration modes were consistent with experimental measurements.

4. CONSTRUCTION OF THE COMBINED OCCUPANT-SEAT MODEL

The interaction at the occupant-seat interfaces affected the pressure distribution and body posture.[25] The contact between the feet with the footrest, the buttocks with the cushion, and the upper body with the backrest, were set to "surface to surface".[17] The penalty function was selected to define the contact characteristics of the occupant-seat interface. The tangential contact behavior was defined as frictional contact, and dynamic and static friction coefficients were defined as 0.3 and 0.2. The normal contact behavior was defined as hard contact (Fig 6). The combined model was further calibrated by the static pressure distribution on the seat from the measurement (Figs. 7 a and 7 b). The peak pressure at the backrest appeared at the shoulder and the protruding part of the spine. The peak pressure at the seat cushion appeared below the ischial tuberosities. The pressure around the peak point showed a uniform decreasing trend. The predicted static pressure distribution was consistent with previous studies.[16,17,23]

The vertical vibration was applied to further calibrate the model with the measured dynamic pressure distribution. The predicted dynamic pressure distribution showed a significant increase in pressure concentration occurring at the backrest and the seat cushion (Figs. 7 c and 7 d). This phenomenon could be caused by the pitching and the vertical movement of the body.[16,17,23]

5. OPTIMIZATION AND APPLICATION OF THE MODEL

5.1. Model Prediction and Sensitivity Analysis

The seat transmissibility could be mainly divided into the vertical inline (v-v) and fore-and-aft cross-axis (v-h) transmissibilities during the exposure to the vertical vibration, and both the seat transmissibilities from the floor to the seat cushion were predicted by the calibrated combined model with the foam thickness set as 80 mm. Although the predicted seat transmissibilities matched the measured data at the primary resonance, there were evident differences at the low frequency range (see Fig. 8). Sensitivity analysis was utilized to assess the key parameters influencing the prediction of the model. The material parameters (the stiffness, the damping, the shear modulus, the density and the Young's modulus) and the contact parameters (the friction coefficient and the contact stiffness) were chosen as the initial variables. The single-factor analysis was applied, and the sensitivity analysis was performed with seven parameters distributed across three levels (0 %, $\pm$30 %). The sensitivity analysis showed the peak frequency of the predicted seat transmissibility decreased with decreased foam stiffness, shear modulus, Young's modulus, density, friction coefficient and contact stiffness, while the peak frequency increased with a decreased foam damping (Fig. 9 a). The peak

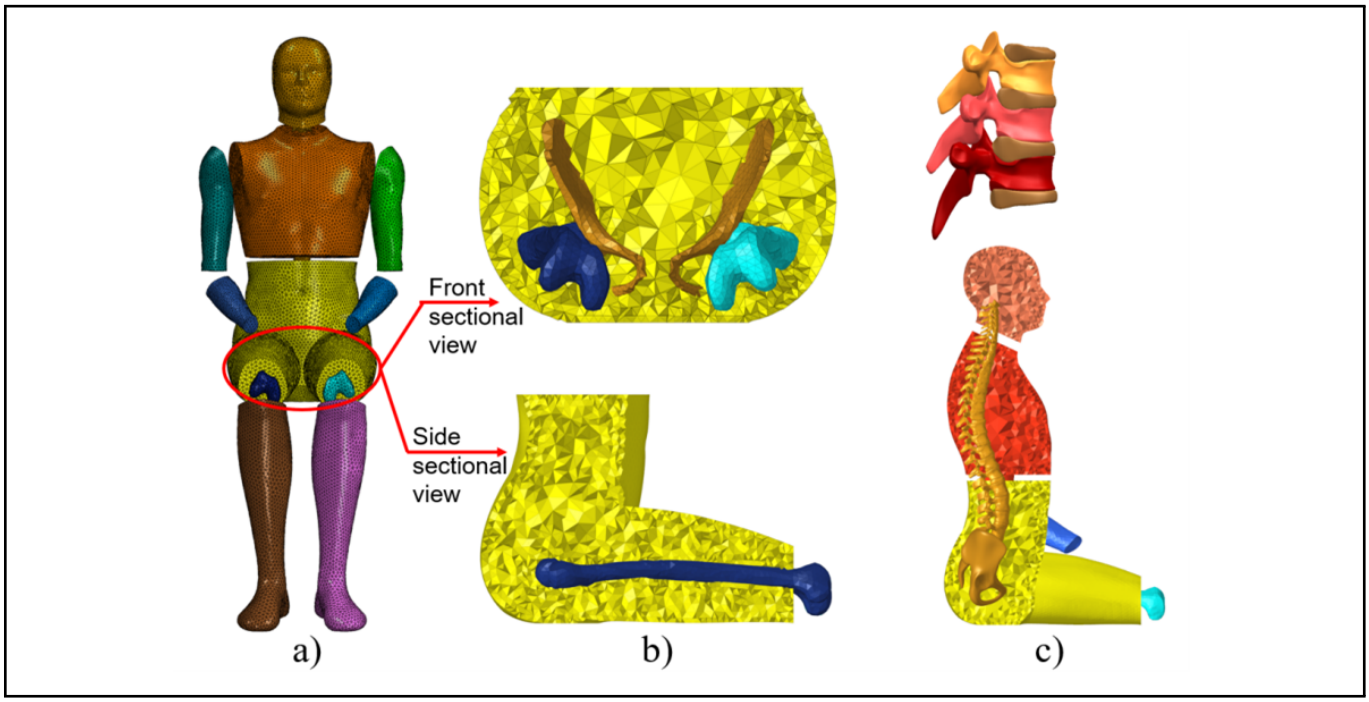

Figure 4. Finite element models: (a) the human body; (b) the frontal and lateral sectional views of the buttocks; (c) the skeletal segments at the occupant-seat interface.

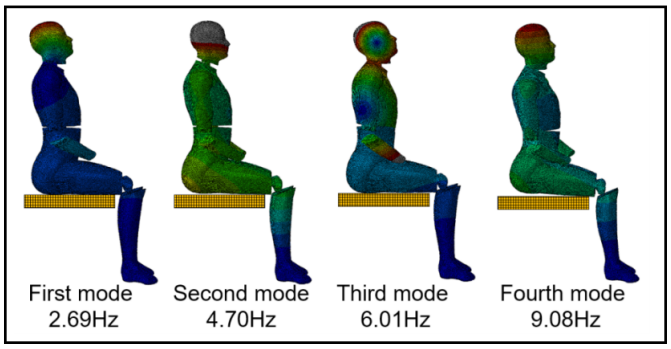

Figure 5. Vibration modes of seated human body.

transmissibility of the predicted seat transmissibility increased with decreased foam stiffness, damping, Young's modulus and shear modulus, while the peak transmissibility decreased with decreased foam density, contact stiffness and the friction coefficient (Fig. 9 b). Furthermore, the influence weightings of the parameters showed damping, shear modulus, stiffness, and Young's modulus of the foam had a greater impact than the other parameters. Therefore, these parameters were selected to be further optimized.

5.2. Optimization with the Polynomial Fitting and the Genetic Algorithm

The third-order polynomial functions were chosen to fit the mapping functions between the model parameters and the peak frequency, and the optimal polynomial coefficients were obtained with the least squares method. The formula is presented below:

$$F = m * (x)^3 + n * (x)^2 + p(x) + q; \tag{9}$$

where x and F represent the range of parameter variation and the peak transmissibility, and m, n, p and q are the fitting parameters. The scatter data and the fitted curves corresponding to each polynomial function are illustrated in Fig. 10. The best fit and the fitting parameters are illustrated in Table 3.

Table 3. The damping and stiffness of joints.

Parameter	Fitting parameters				Goodness of fit
	m(e-5)	n(e-3)	p	q	
Damping	19.9	-1.5	-1.5	0.20	0.99242
Young's modulus	-3.0	-2.7	0.9	-0.03	0.99992
Shear modulus	-3.0	-2.7	0.9	-0.03	0.99992
Density	5.3	-0.3	0.2	-0.44	0.77823
Stiffness	-3.0	-2.7	0.9	-0.03	0.99992
Contact stiffness	4.3	-0.3	0.1	-0.38	0.77745
Frictional coefficient	4.3	0.5	0.2	0.74	0.71926

The mapping functions were combined to construct a prediction function as follows:

$$f_{red}(p1, p2, p3, p4) = \\ w_1 f_1(p_1) + w_2 f_2(p_2) + w_3 f_3(p_3) + w_4 f_4(p_4); \tag{10}$$

where $f_i(p_i)$ represents the fitting functions of the foam damping, foam stiffness, Young's modulus, and the shear modulus. The weight coefficients w_i were determined based on the sensitivity analysis. Specifically, the w_1 (damping) was set as 0.276, and the w_2 (stiffness), w_3 (Young's modulus) and w_4 (shear modulus) were set as 0.241. The squared error (SE) was set as the objective function:

$$SE = (f_{red}(p1, p2, p3, p4) - f_{meas})^2 \tag{11}$$

where f_{meas} represents the measured seat transmissibility. The objective function was optimized with a genetic algorithm to find the optimal values of the key parameters. The new offspring were generated with the intermediate crossover strategy, and the crossover probability was defined as 0.8. The model parameters were subjected to the random perturbations through the adaptive feasible mutation. Furthermore, the size of the population and generation count was defined as 200 and 300.

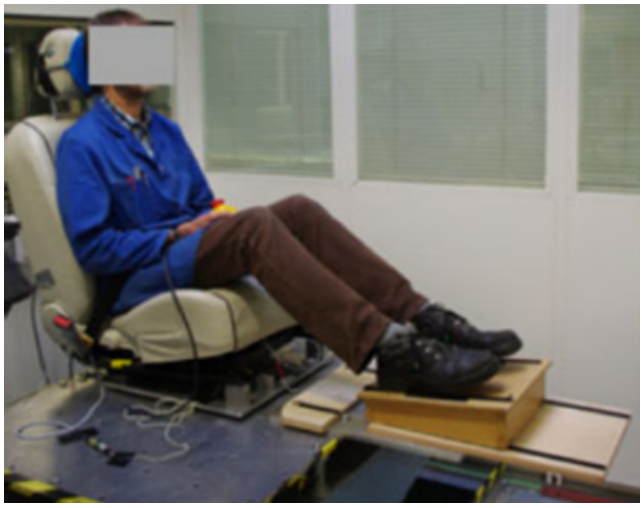

(a) Experimental setup

(b) Combined model

Figure 6. Vibration modes of seated human body.

5.3. Prediction Of Seat Transmissibilities with the Optimized Model

The comparison between the measured and the predicted seat transmissibilities is illustrated in Fig. 11 (foam thickness: 80 mm). The predicted v-v and v-h seat transmissibilities of the original model exhibited peak frequencies at about 4.2 Hz and 3.92 Hz, respectively. The predicted v-v and v-h seat transmissibilities of the optimized model exhibited peak frequencies at about 4.16 Hz and 3.93 Hz, respectively. The SE of the v-v and v-h seat transmissibilities of the original model were 0.0484 and 0.1444, while the SE of the optimized model decreased by 0.0459 and 0.1248, respectively. The goodness of fit for the original model to predict the v-v and the v-h seat transmissibilities was 72.08 % and 69.35 %, with fitting errors of 1.508 and 2.626, respectively. The predicted goodness of fit for the optimized model increased by 13.34 % and 14.41 %, and the fitting errors decreased by 44.9 % and 65.2 %, respectively. The prediction of the optimized model and the measurement showed a high degree of fit with each other. Similar predictive accuracy was achieved when the foam thickness was set as 60 and 100 mm. In addition, the optimized model achieves improved prediction accuracy while maintaining acceptable computational times, as the necessary structural simplifications were applied during the modeling process.

Table 4. Objective evaluation index for the dynamic riding discomfort.

Direction	Objective index	Foam thickness		
		60 mm	80 mm	100 mm
v–v	Peak frequency	4.11	3.93	3.75
	Peak transmissibility	1.99	2.31	2.45
	SEAT value	94.26 %	80.44 %	70.79 %
v–h	Peak frequency	4.69	4.17	3.30
	Peak transmissibility	0.39	0.52	0.58
	SEAT value	98.24 %	86.23 %	79.44 %
Total	WRMSA	0.3942 m/s^2	0.3086 m/s^2	0.2847 m/s^2
	Comfort level	a little uncomfortable	not uncomfortable	not uncomfortable

The peak frequency decreased with increased foam thickness, while the peak transmissibility showed an increased trend (Fig. 12). This trend was consistent with previous experimental findings.[16,17,23]

5.4. Analysis of the Objective Indicators with Optimized Model

Based on the predicted acceleration at the occupant-seat surfaces, the WRMSA and the SEAT value could be further computed to evaluate the predictive accuracy of the model. The WRMSA for each axis is calculated as below:

$$a_w = \left[\int_{f_i}^{f_u} W^2(f)\, G_a(f)\, df\right]^{\frac{1}{2}}; \tag{12}$$

where f_1 and f_u represent the weighted frequency range, the $W(f)$ represents the frequency weighting, and the $G_a(f)$ denotes the acceleration power spectral density. The total WRMSA can be calculated as follows:

$$a_v = \left(k_x^2 a_{wx}^2 + k_y^2 a_{wy}^2 + k_z^2 a_{wz}^2\right)^{\frac{1}{2}}; \tag{13}$$

where k_x, k_y, k_z and a_{wx}, a_{wy}, a_{wz} represent the weighting coefficients and the WRMSA in each axis, respectively. The weighting curve $W(f)$ was selected based on the frequency weighting corresponding to the sensitivity of different body parts.

The SEAT value was obtained based on the WRMSA[31] and calculated as:

$$\text{SEAT} = \left[\frac{A_{w(\text{seat})}}{A_{w(\text{base})}}\right] \cdot 100; \tag{14}$$

where $A_{w(\text{seat})}$ and $A_{w(\text{base})}$ represent the WRMSA of the cushion and the seat base.

The comfort level could be evaluated by comparing the total WRMSA with the discomfort range given in the ISO 2631-1. As shown in Table 4, the predicted total WRMSA decreased with increased foam thickness. The comfort level corresponding to the WRMSA improved from "a little uncomfortable" to "not uncomfortable" with increased foam thickness. Furthermore, the measured WRMSA were 0.41105 m/s^2, 0.31385 m/s^2 and 0.29643 m/s^2 with the foam thickness set as 60 mm, 80 mm and 100 mm, respectively. Both the variation trend and the corresponding comfort level of the predicted data were similar to the measured data.

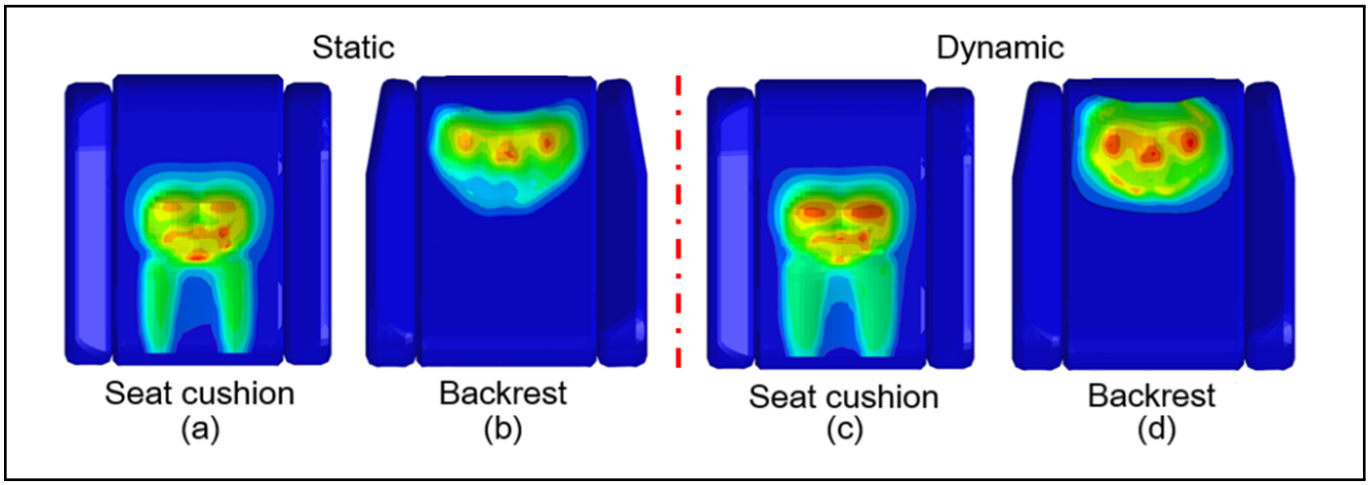

Figure 7. The pressure distribution.

The predicted vertical and fore-and-aft SEAT values reached the maximum when the foam thickness was 60 mm, and the SEAT values decreased with increased foam thickness. Although the 60 mm foam could provide vibration isolation as well, its performance was relatively poor. The objective index results suggest that the SEAT values in both the vertical in-line and the fore-and-aft cross-axis direction were reduced by 13.82 % (from 94.26 % to 80.44 %) and 12.01 % (from 98.24 % to 86.23 %), when the foam thickness increased from 60 mm to 80 mm, whereas the reductions diminished to 9.65 % (from 80.44 % to 70.79 %) and 6.79 % (from 86.23 % to 79.44 %) when the thickness was further increased from 80 mm to 100 mm. These results demonstrate that the change ratio of the predicted SEAT values decreased with increased foam thickness.[5] Moreover, the change ratio of the predicted SEAT values decreased with increased foam thickness, indicating the improvement of the riding comfort exhibited diminishing returns with increasing the foam thickness.

The predicted peak transmissibility of the v-v and v-h seat transmissibilities increased with increased foam thickness, thereby increasing the discomfort by vibrations.[32] However, the peak frequencies of the v-v and v-h seat transmissibility decreased to below 4 Hz when the foam thickness reached 80 mm and 100 mm, which were far from the sensitive frequency range of the human body ($4-8$ Hz),[33] thereby enhancing the vibration tolerance of the seat system and improving the dynamic riding comfort.[34] The increase in the total WRMSA and the SEAT value also showed an improvement in the overall comfort. Thus, the resonance should be avoided when increasing the foam thickness to enhance the comfort.

6. CONCLUSION

A finite element model of the seated human body including the spine, the pelvis, the femur and the muscle tissues was constructed to predict the seat transmissibility and the cross-axis effect with different foam thicknesses during the whole-body vibration. Construction of the skeletal structures (e.g. the spine and the pelvis) and calibrations of the human body model with the vibration modes could improve the capability of predicting the cross-axis effect of the occupant-seat system. Calibration of the vibration transmission through interfaces between the seat and the human body with measured static and dynamic pressure distributions could enhance the accuracy and stability of the combined occupant-seat model. The parameter optimization method that combined the sensitivity analysis, the polynomial fitting and the genetic algorithm could significantly enhance the prediction performance of the model for the whole-body vibration response. The model parameters were established and calibrated based on the GB 10000-88. Future research is necessary to extend the findings to a broader range of body sizes. Since cross-axis responses and muscle activities differ during the exposure to various excitations, corresponding experiments are required to calibrate and validate the model for transient or non-vertical vibration excitations.

REFERENCES

[1] Dong, R., Zhu, S., Cheng, X., Gao, X., Wang, Z. and Wang, Y. Study on the biodynamic characteristics and internal vibration behaviors of a seated human body under biomechanical characteristics, *Biomechanics and Modeling in Mechanobiology*, **23**, 1449–1468, (2024). https://doi.org/10.1007/s10237-024-01849-z

[2] Mondal, P. and Arunachalam, S. Unique finite element modelling of human body inside accelerating car to predict accelerations and frequencies at different human segments, *Applied Sciences*, **10**, 1861, (2020). https://doi.org/10.3390/app10051861

[3] Zhao, Y., Bi, F., Shu, H., Guo, L. and Wang, X. Prediction of the driver's head acceleration and vibration isolation performance of the seating suspension system using the time and frequency domain modeling, *Applied Acoustics*, **183**, 108308, (2021). https://doi.org/10.1016/j.apacoust.2021.108308

[4] Mansfield, N. J., Holmlund, P., Lundstrom, R., Lenzuni, P. and Nataletti, P. Effect of vibration magnitude, vibration spectrum and muscle tension on apparent mass and cross axis transfer functions during whole-body vibration exposure, *Journal of Biomechanics*, **39**, 3062–3070, (2006). https://doi.org/10.1016/j.jbiomech.2005.09.024

[5] Zhang, X., Qiu, Y. and Griffin, M. J. Transmission of vertical vibration through a seat: effect of thickness of

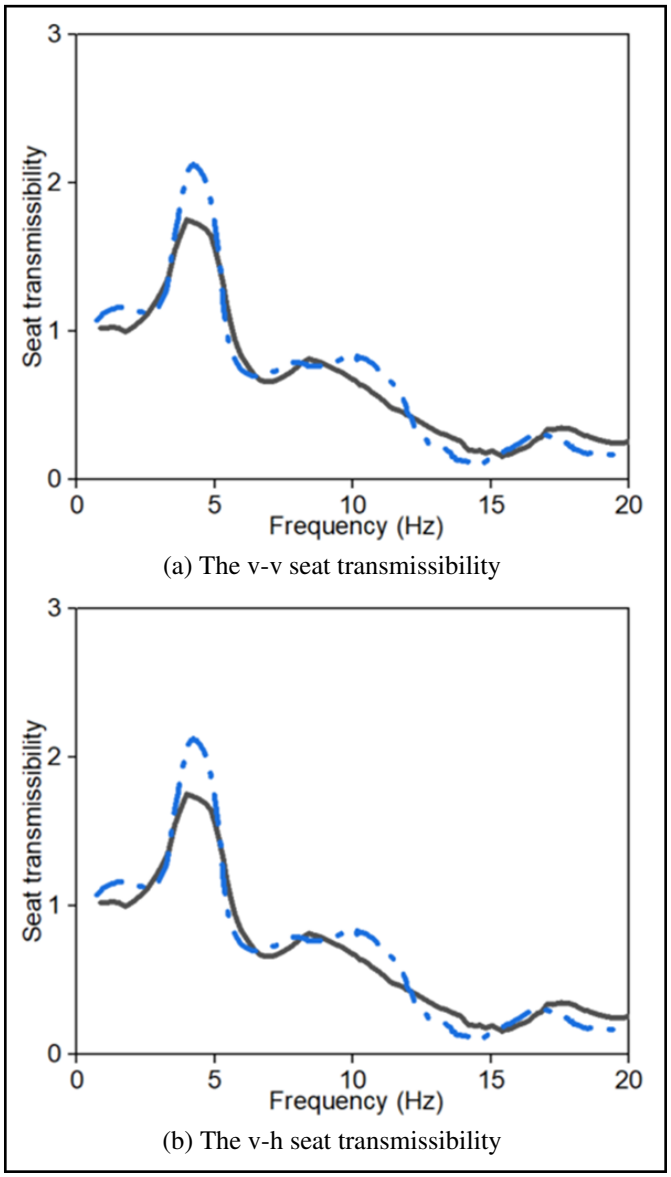

(a) The v-v seat transmissibility

(b) The v-h seat transmissibility

Figure 8. Comparison between the predicted and measured seat transmissibilities (foam thickness: 80 mm): ——measurement; - · - · prediction.

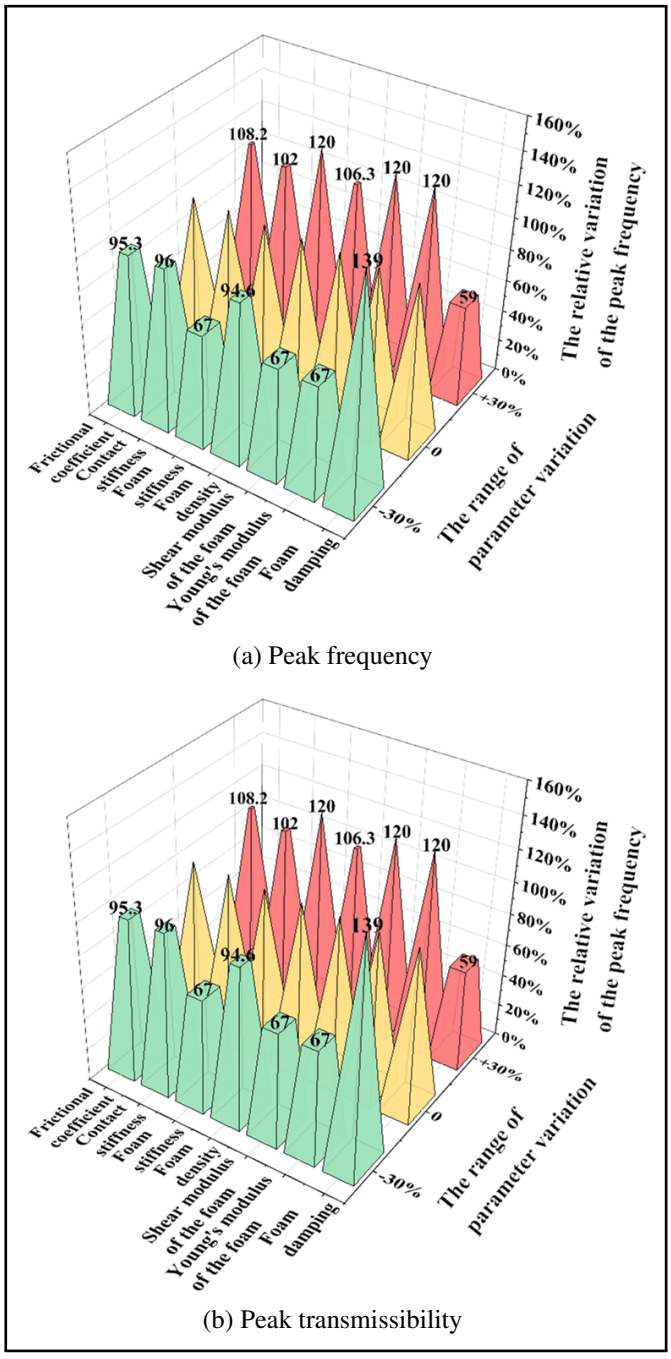

(a) Peak frequency

(b) Peak transmissibility

Figure 9. Sensitivity analysis of model parameters.

foam cushions at the seat pan and the backrest, *International Journal of Industrial Ergonomics*, **48**, 36–45, (2015). https://doi.org/10.1016/j.ergon.2015.03.006

[6] Zhang, X., Qiu, Y. and Griffin, M. J. Developing a simplified finite element model of a car seat with occupant for predicting vibration transmissibility in the vertical direction, *Ergonomics*, **58**, 1220–1231, (2015). https://doi.org/10.1080/00140139.2015.1005165

[7] Barbeau, R., Weisser, T., Dupuis, R., Aubry, É. and Baudu, S. Assessment of the impact of sub-components on the dynamic response of a coupled human body/automotive seat system, *Journal of Sound and Vibration*, **459**, 114846, (2019). https://doi.org/10.1016/j.jsv.2019.07.012

[8] Kim, D. Y., Bang, J. H., Lee, C. A., Kim, H. Y., Choi, K. Y. and Lim, B. G. Numerical evaluation of time-dependent sagging for low density polyurethane foams to apply the long-term driving comfort on the seat cushion design, *International Journal of Industrial Ergonomics*, **64**, 178–187, (2018). https://doi.org/10.1016/j.ergon.2016.08.010

[9] Kolich, M., Essenmacher, S. D. and Mcevoy, J. T. Automotive seating: the effect of foam physical properties on occupied vertical vibration transmissibility, *Journal of Sound and Vibration*, **281**, 409–416, (2005). https://doi.org/10.1016/j.jsv.2004.03.058

[10] Pan-Zagorski, W., Johnson, P. W., Pereny, M. and Kim, J. H. Automotive seat comfort and vibration performance evaluation in dynamic settings, *Applied Sciences*, **12**, 4033, (2022). https://doi.org/10.3390/app12084033

[11] Kitazaki, S. and Griffin, M. J. Resonance behaviour of the seated human body and effects of posture,

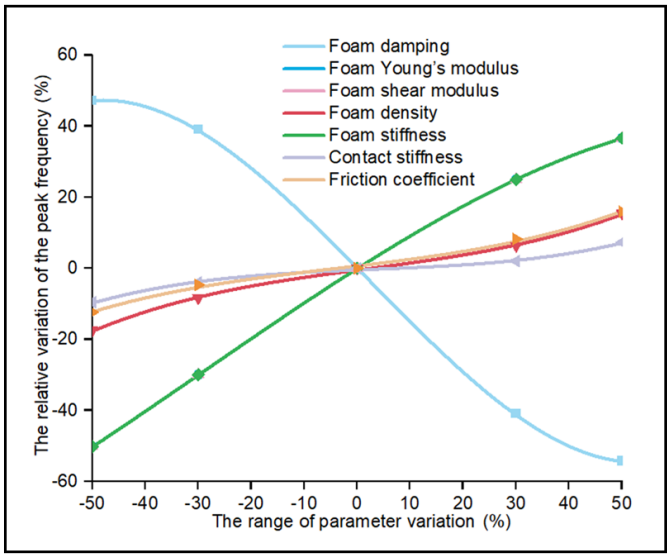

Figure 10. The scatter data and the fitted curves.

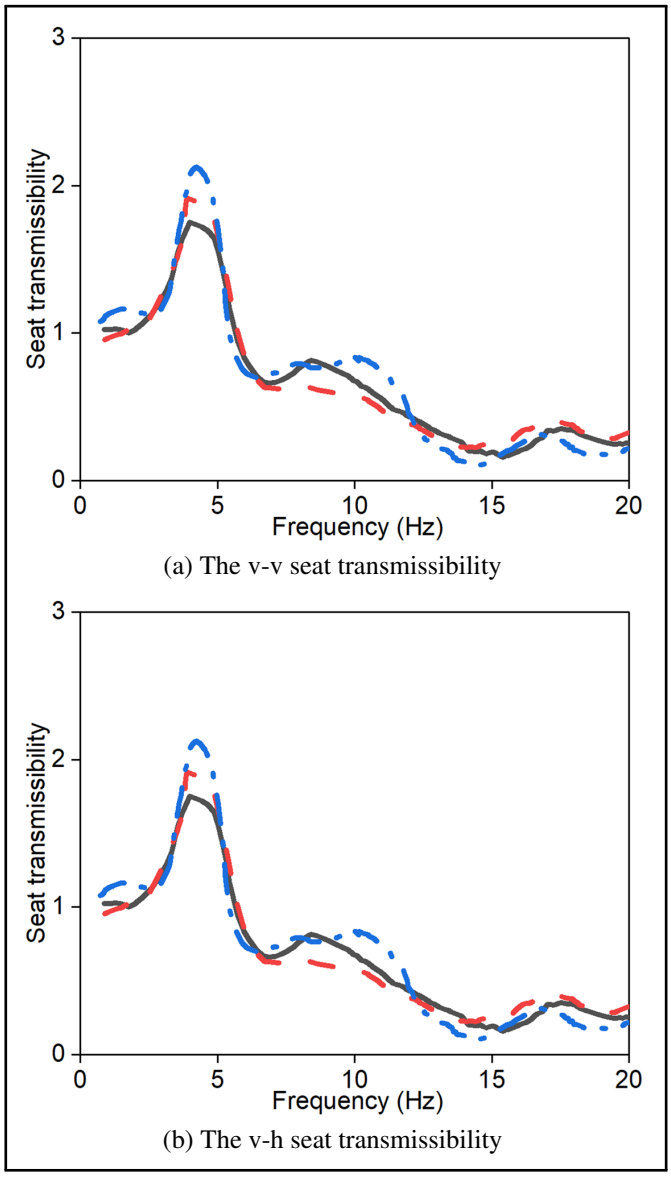

Figure 11. Comparison between the measured and predicted seat transmissibilities (foam thickness: 80 mm): ——measured, -·-·-predicted from the original model, - - -predicted from the optimized model.

Journal of Biomechanics, **31**, 143–149, (1998). https://doi.org/10.1016/S0021-9290(97)00126-7

[12] Zheng, G., Qiu, Y. and Griffin, M. J., An analytic model of the in-line and cross-axis apparent mass of the seated human body exposed to vertical vibration with and without a backrest, *Journal of Sound and Vibration*, **330**, 6509–6525, (2011). https://doi.org/10.1016/j.jsv.2011.06.026

[13] Sun, C., Qiu, Y., Liu, C., Zheng, X., Wu, J. and Zhang, X. Experimental modal analysis of the seated human body during whole-body vibration: effect of vibration direction and magnitude, *Journal of Low Frequency Noise, Vibration and Active Control*, **43**, 1654–1671, (2024). https://doi.org/10.1177/14613484241258103

[14] Zhao, L., Yu, Y., Cao, J. and Zhou, W. Nonlinear coupled dynamic modelling of driver-seat-cab system and biomechanical behaviour prediction, *Strojniški Vestnik*, **68**, 90–100, (2022). https://doi.org/10.5545/sv-jme.2021.7429

[15] Wu, J. and Qiu, Y. Modeling and analysis of a train seat with occupant exposed to combined lateral, vertical and roll vibration, *Journal of Sound and Vibration*, **496**, 115920, (2021). https://doi.org/10.1016/j.jsv.2020.115920

[16] Siefert, A., Pankoke, S. and Wölfel, H. P. Virtual optimisation of car passenger seats: simulation of static and dynamic effects on drivers' seating comfort, *International Journal of Industrial Ergonomics*, **38**, 410–424, (2008). https://doi.org/10.1016/j.ergon.2007.08.016

[17] Yadav, S. K., Huang, C., Mo, F., Li, J., Chen, J. and Xiao, Z. Analysis of seat cushion comfort by employing a finite element buttock model as a supplement to pressure measurement, *International Journal of Industrial Ergonomics*, **86**, 103211, (2021). https://doi.org/10.1016/j.ergon.2021.103211

[18] Verver, M. M., van Hoof, J., Oomens, C. W. J., Wismans, J. S. H. M. and Baaijens, F. P. T. A finite element model of the human buttocks for prediction of seat pressure distributions, *Computer Methods in Biomechanics and Biomedical Engineering*, **7**, 193–203, (2004). https://doi.org/10.1080/10255840410001727832

[19] Kim, E., Fard, M. and Kato, K. A seated human model for predicting the coupled human-seat transmissibility exposed to fore-aft whole-body vibration, *Applied Ergonomics*, **84**, 102929, (2020). https://doi.org/10.1016/j.apergo.2019.102929

[20] Liu, C., Qiu, Y. and Griffin, M. J. Finite element modelling of human-seat interactions: vertical in-line and fore-and-aft cross-axis apparent mass when sitting on a rigid seat without backrest and exposed to vertical vibration, *Ergonomics*, **58**, 1207–1219, (2015). https://doi.org/10.1080/00140139.2015.1005164

[21] Kauraw, V., Chaupal, P. and Rajendran, P. Vibration analysis of human body under seating posture: an automobile application, *Journal of the Brazilian Society of*

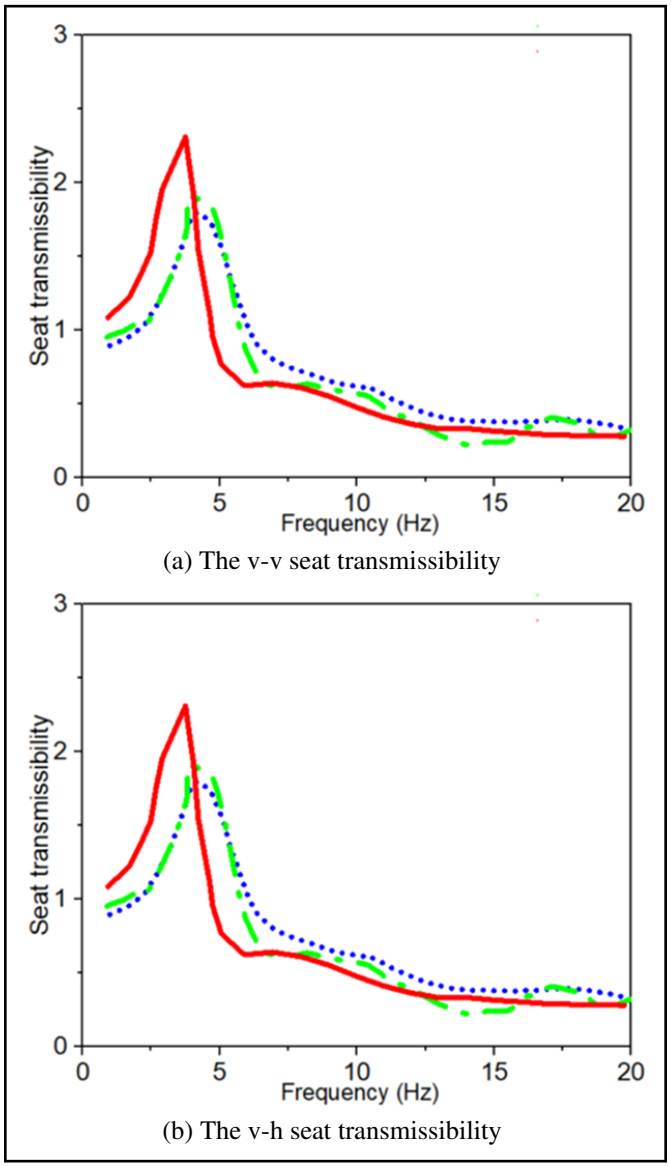

(a) The v-v seat transmissibility

(b) The v-h seat transmissibility

Figure 12. The effect of different foam thicknesses on the seat transmissibility predicted by the optimized model: ····· 60 mm, -·-·- 80 mm, —— 100 mm.

Mechanical Sciences and Engineering, **45**, 200, (2023). https://doi.org/10.1007/s40430-023-04119-8

[22] Luo, Q., He, Y., Zhang, Z. and Gao, K. Transmission of vertical vibration through a seat cushion at the seat pan: effect of foam physical properties during different excitation magnitudes, *Journal of Low Frequency Noise, Vibration and Active Control*, **43**, 144–155, (2024). https://doi.org/10.1177/14613484231197985

[23] Huang, S., Zhang, Z., Xu, Z. and He, Y. Modeling of human model for static pressure distribution prediction, *International Journal of Industrial Ergonomics*, **50**, 186-195, (2015). https://doi.org/10.1016/j.ergon.2015.09.017

[24] Desai, R., Guha, A. and Seshu, P. Modelling and simulation of an integrated human-vehicle system with non-linear cushion contact force, *Simulation Modelling Practice and Theory*, **106**, 102206, (2021). https://doi.org/10.1016/j.simpat.2020.102206

[25] Dong, R., He, L., Du, W., Cao, Z. and Huang, Z. Effect of sitting posture and seat on biodynamic responses of internal human body simulated by finite element modeling of body-seat system, *Journal of Sound and Vibration*, **438**, 543–554, (2019). https://doi.org/10.1016/j.jsv.2018.09.012

[26] Guo, L. and Zhang, C. Development and validation of a whole human body finite element model with detailed lumbar spine, *World Neurosurgery*, **163**, e579–e592, (2022). https://doi.org/10.1016/j.wneu.2022.04.037

[27] Grujicic, M., Pandurangan, B., Arakere, G., Bell, W. C., He, T. and Xie, X. Seat-cushion and soft-tissue material modeling and a finite element investigation of the seating comfort for passenger-vehicle occupants, *Materials & Design*, **30**, 4273–4285, (2009). https://doi.org/10.1016/j.matdes.2009.04.028

[28] Wu, J., Qiu, Y. and Chao, S. Modelling and analysis of coupled vibration of human body in the sagittal and coronal planes exposed to vertical vibration, *Mechanical Systems and Signal Processing*, **166**, 108439, (2022). https://doi.org/10.1016/j.ymssp.2021.108439

[29] Gao, K., Li, C. and Xiao, Y. Finite element modeling and parameter identification of the seated human body exposed to vertical vibration, *Biomechanics and Modeling in Mechanobiology*, **20**, 1789–1803, (2021). https://doi.org/10.1007/s10237-021-01481-1

[30] Gao, K., Zhang, Z., Luo, L. and He, Y. Evaluation of subjective discomfort of the seated human body exposed to vertical vibration using dynamic body pressure, *Journal of Low Frequency Noise, Vibration and Active Control*, **42**, 438–451, (2023). https://doi.org/10.1177/14613484221130336

[31] Sharma, A. and Mandal, B. B. Attenuation of mechanical vibration during transmission to human body through mining vehicle seats, *Mining, Metallurgy & Exploration*, **38**, 1449–1461, (2021). https://doi.org/10.1007/s42461-021-00406-x

[32] Zhang, X., Zhang, Q., Li, Y., Liu, C. and Qiu, Y. Effect of the thickness of polyurethane foams at the seat pan and the backrest on fore-and-aft in-line and vertical cross-axis seat transmissibility when sitting with various contact conditions of backrest during fore-and-aft vibration, *Applied Ergonomics*, **93**, 103354, (2021). https://doi.org/10.1016/j.apergo.2021.103354

[33] Cvok, I., Hrgetić, M., Hoić, M., Deur, J. and Ivanovic, V. Design of a linear motor-based shaker rig for testing driver's perceived ride comfort, *Mechatronics*, **75**, 102521, (2021). https://doi.org/10.1016/j.mechatronics.2021.102521

[34] Wu, J. and Qiu, Y. Analysis of ride comfort of high-speed train based on a train-seat-human model in the vertical direction, *Vehicle System Dynamics*, **59**, 1867–1893, (2021). https://doi.org/10.1080/00423114.2020.1794014